photonics

MDPI

Communication

Multi-Bessel Beams Generated by an Axicon and a Spatial Light Modulator for Drilling Applications

Christian Lutz [1,*], Simon Schwarz [1], Jan Marx [2], Cemal Esen [2] and Ralf Hellmann [1]

[1] Applied Laser and Photonics Group, University of Applied Sciences Aschaffenburg, Würzburgerstraße 45, 63743 Aschaffenburg, Germany
[2] Applied Laser Technologies, Ruhr University Bochum, Universitätsstraße 150, 44801 Bochum, Germany
* Correspondence: christian.lutz@th-ab.de

Abstract: We report on an optical setup to generate multi-Bessel beam profiles combining a refractive axicon and a spatial light modulator. Based on their particular beam profile, Bessel beams offer advantageous properties for micro drilling processes and internal volume processing, especially for transparent materials. In addition, the laser power of industrial, ultrashort pulsed lasers has increased significantly over the last few years, offering the possibility for highly efficient processes using multi-spot profiles. Our optical concept combines the dynamic possibilities of beam splitting using a spatial light modulator with the benefits of Bessel beams, which facilitates multi-Bessel beam processing. Beside the simulation and experimental evaluation of the generated multi-Bessel beams, we exemplify the applicability of the developed module for the perforation of thin metal foils by micro drilling.

Keywords: Bessel beam; axicon; optical system; ultrashort pulsed laser; material ablation

Citation: Lutz, C.; Schwarz, S.; Marx, J.; Esen, C.; Hellmann, R. Multi-Bessel Beams Generated by an Axicon and a Spatial Light Modulator for Drilling Applications. *Photonics* **2023**, *10*, 413. https://doi.org/10.3390/photonics10040413

Received: 14 March 2023
Revised: 3 April 2023
Accepted: 3 April 2023
Published: 6 April 2023

1. Introduction

Diffraction-free Bessel beams were first discovered and described by Durnin et al. [1] in 1987, and they represent the propagation-invariant solution of the Helmholz equation. While Durnin et al. [2] showed convergences to the ideal Bessel beams for a finite range, in theory, they are of an infinite transverse extent and they carry infinite energy, so they cannot be generated experimentally [3,4]. To design a so-called quasi-Bessel beam, based on a Gaussian beam profile, there are several commonly used components, such as ring apertures [2], binary-coded holograms [5], axicon lenses [6,7], converging lenses with spherical aberrations [8], tunable acoustic gradient lenses [9], phase-shifted Fresnel axicons [10], and spatial light modulators (SLMs) [11,12], respectively, which have been successfully employed. Using a SLM, it is also possible to create an array of Bessel beams with a flexible separation instead of a single Bessel beam [13–15].

Quasi-Bessel beams offer advantages for various micro-machining processes due to their particular intensity distribution. The long and high intensity range in the propagation direction of a quasi-Bessel beam makes it an excellent tool, especially for laser drilling holes with a high aspect ratio in transparent materials. As Xie et al. [4] showed, the advantage of the higher focal length of Bessel beams leads to a 52 times higher aspect ratio as compared to a focused Gaussian beam profile. With a further improvement of the focal position and the used pulse energy, the authors achieved an aspect ratio of up to 330:1 in PMMA, for holes with a diameter between 1.5 µm and 2.4 µm. In addition to drilling holes in transparent materials, Bessel beams offer the possibility to induce cracks in glass in a controlled manner by means of internal volume modification. For example, Dudutis et al. [16] demonstrated the possibility of using a pulse energy of 2 mJ to produce a 2.3 mm-long modification of an elliptical shape to create cracks in the axial direction. Finally, it was shown that it is possible to control the orientation of the cracks by rotating the polarization of the Bessel

beam profile. Furthermore, Mitra et al. [17] fabricated nanovoids with a length up to 5 mm in borosilicate glass, corresponding to an aspect ratio of 1200:1.

While the processing of transparent materials is often possible with one or a few pulses [4], the processing of non-transparent materials, such as metals, requires a large number of pulses, due to the significantly smaller optical penetration depth. According to Alexeev et al. [18], the aspect ratio of holes drilled by a Bessel beam in non-transparent materials is significantly lower, as exemplified by this for drilling 100 µm-thick copper sheets with an exit hole diameter of 15 µm. Due to the typical Bessel beam profile, which is also characterized by ring-shaped intensities around the intense maximum, ring-shaped modifications or even ablation can be seen on the processed surface of non-transparent materials [18]. To minimize these effects, He et al. [19] developed a tailored Bessel beam using a binary phase plate in front of the axicon, which enables the drilling of 6 µm holes in a 100 µm silicon wafer.

The most common method of creating a quasi-Bessel beam for drilling applications is to use an axicon in combination with an imaging lens assembly [3,16,20,21]. Although this allows processes with low power losses and high-quality drilled holes, it only generates one single Bessel beam. Additionally, the generation of Bessel beam arrays is a promising method for drilling applications with multi-spot beam profiles [22]. Contrary to conventional axicons, which generate one quasi-Bessel beam behind their apex, axicon arrays can be used to form a multitude of these beams. Schwarz et al. [23] showed a femtosecond laser ablation process with a polishing step using a CO_2 laser for the production of micro axicon arrays, including a characterization of the resulting multi-Bessel beams. While axicon arrays have a fixed separation of the Bessel beams due to their fixed geometry, the separation of the Bessel beams can be adapted to the machining process using variable optical elements.

Spatial light modulators are variable optical elements for a lot of different beam-shaping applications, such as spherical aberration correction [24] and multi-spot processing [25]. By means of SLM, it is possible to create multi-Bessel beams by combining axicon phase patterns or beam splitter functions [26–28]. Studies by García-Martínez et al. [26] show the generation of multi-Bessel beams by a combination of phase patterns consisting of linear axicons or binary axicons with a Dammann grating, resulting in a focal depth of more than 125 cm. The limited phase shift of an SLM allows only very small axicon angles compared to commercial axicons made of glass, resulting in very long Bessel beams of several centimeters or even meters in length [26,29].

Reducing the period length of the phase mask imaged on the SLM results in a larger angle, but the diffraction efficiency of the SLM decreases drastically, and efficient operation with this setup is not possible due to high power losses. Based on these correlations, in this contribution we demonstrate an optical system based on a simulation and experimental evaluation that combines the flexible beam-shaping capabilities of an SLM with an axicon-generated Bessel beam profile to create multi-Bessel beams. The SLM enables flexible changes of the Bessel beam separation by the calculated computer-generated hologram without the exchange of optical components and subsequent adjustment work on the optical setup. This approach allows the drilling of holes in non-transparent materials using a multi-Bessel beam, which is exemplified by an experimental study of a multi-Bessel beam.

2. Experimental

We used an ultrashort pulsed laser (Light Conversion, Pharos, Vilnius, Lithuania) with a wavelength of 1028 nm, an adjustable repetition rate of up to 610 kHz, and a pulse duration between 230 fs and 15 ps. The linearly polarized and collimated laser beam with a diameter of 3.4 mm (FWHM) is shaped by a Holoeye SLM (Berlin, Germany) with a resolution of 1920 × 1080 pixels with a pixel pitch of 8 µm (Pluto 2, NIR-015-D, Berlin, Germany) in combination with a 170° precision axicon from Eksma Optics (Vilnius, Lithuania) and different lenses to complete the optical setup. After reflecting the laser beam from the SLM, the first lens (f = 100 mm) is placed 200 mm behind the SLM to image its

phase pattern onto the following axicon. Behind the axicon, the resulting Bessel beam is imaged using a 4f-setup with two lenses with f = 100 mm and f = 50 mm into the focal plane. By superimposing the phase pattern of the SLM and the imaged Bessel beam, a multi-Bessel beam results in the focus of lens 3. To image the intensity distribution, a camera (IDS UI-1490SE-M-GL, Farnham, UK) is used, which is replaced by a workpiece in order to conduct experimental drilling applications.

The optical setup shown in Figure 1 allows for the adjustment of the separation of a multi-spot beam profile using the SLM with different beam splitter patterns and the generation of multi-Bessel beams with the included axicon. As stated before, the generation of Bessel beams only using an SLM leads to very long intensity profiles, while this setup combines short Bessel beams generated by the used axicon with the flexibility regarding the beam-splitting possibilities of the SLM.

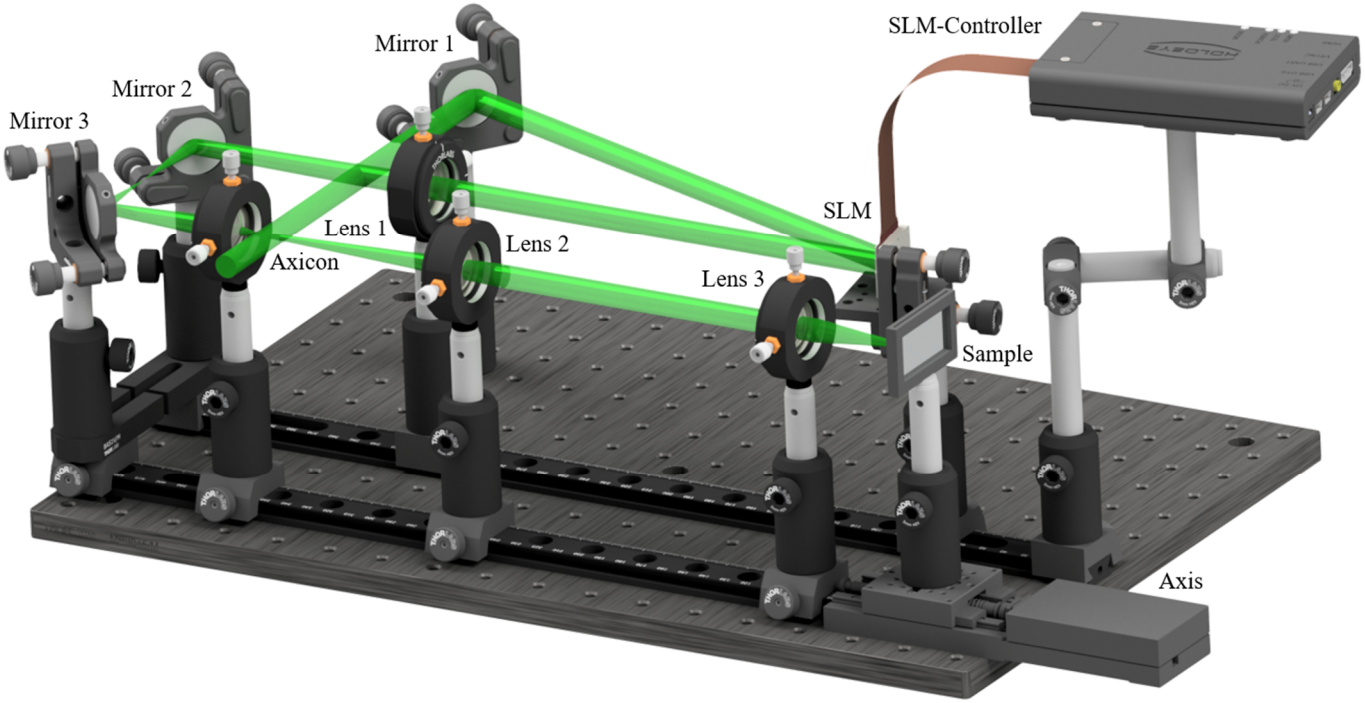

Figure 1. Schematic illustration of the optical system for multi-Bessel beam generation using a spatial light modulator, a 4f-telescope, an axicon, focusing lenses, and an exemplary sample in form of a metal sheet, which can be replaced by a camera for recording the beam profiles.

3. Simulation

To simulate parameters such as the spot separation and the axicon angle, Virtual Lab from LightTrans International GmbH (Jena, Germany) is used. The simulation results in Figure 2 show an optical system that generates multi-Bessel beams with the described combination of a spatial light modulator and an axicon. The input beam is defined as 3.4 mm in diameter ($1/e^2$) with a Gaussian shape, which is directed onto the SLM. The phase pattern shown in Figure 2a is a computer-generated hologram (CGH), which is calculated with an iterative Fourier transform algorithm with a spot separation of 1 mm for a focal length of 100 mm. Thus, at the focal plane between lens 1 and the following axicon, Figure 2b shows a 2 × 2 regular beam splitter with Gaussian-shaped spots and a separation of 1 mm. As a result of the superposition of the phase pattern, in 30 mm distance from the axicon, a multiplied Bessel beam with a separation of 200 µm is shown in Figure 2c. Through the following two lenses, the beam profile is imaged into the focal plane with a separation of 1 mm, where material processing is possible (Figure 2d). Furthermore, the intensity distribution along the propagation direction of the single Bessel beam was simulated. The beam profiles shown in Figure 3 were obtained by detecting the intensity

in the cross-section at different Z propagations: (a) shows the intensity distribution of the beam directly after the axicon with a length of 68.8 mm (FWHM) for a single Bessel beam, while the SLM is treated as a mirror. After a propagation of z = 21 mm, the Bessel beam reaches its maximum intensity and has a core diameter of 15.3 µm (FWHM). The ring-shaped secondary maxima that are typical for Bessel beams can also be seen, which move away from the center of the beam profile with increasing propagation, due to the divergent input beam of the axicon. Through lenses two and three, the beam is imaged according to the focal lengths of the lenses in the ratio 2 to 1. As can be seen in Figure 3b, the diameter at the point of maximum intensity, which is reached at a propagation length of z = 5.2 mm, is halved to 7.6 µm (FWHM). Due to the special propagation properties of Bessel beams, the imaging ratio of 2:1 has a quadratic effect on the length of the intensity distribution [30]. The length of the Bessel beam is thus 17.5 mm. In addition, the ring-shaped side maxima behave accordingly, whereby a higher number can be seen by imaging in the same cross-sectional area.

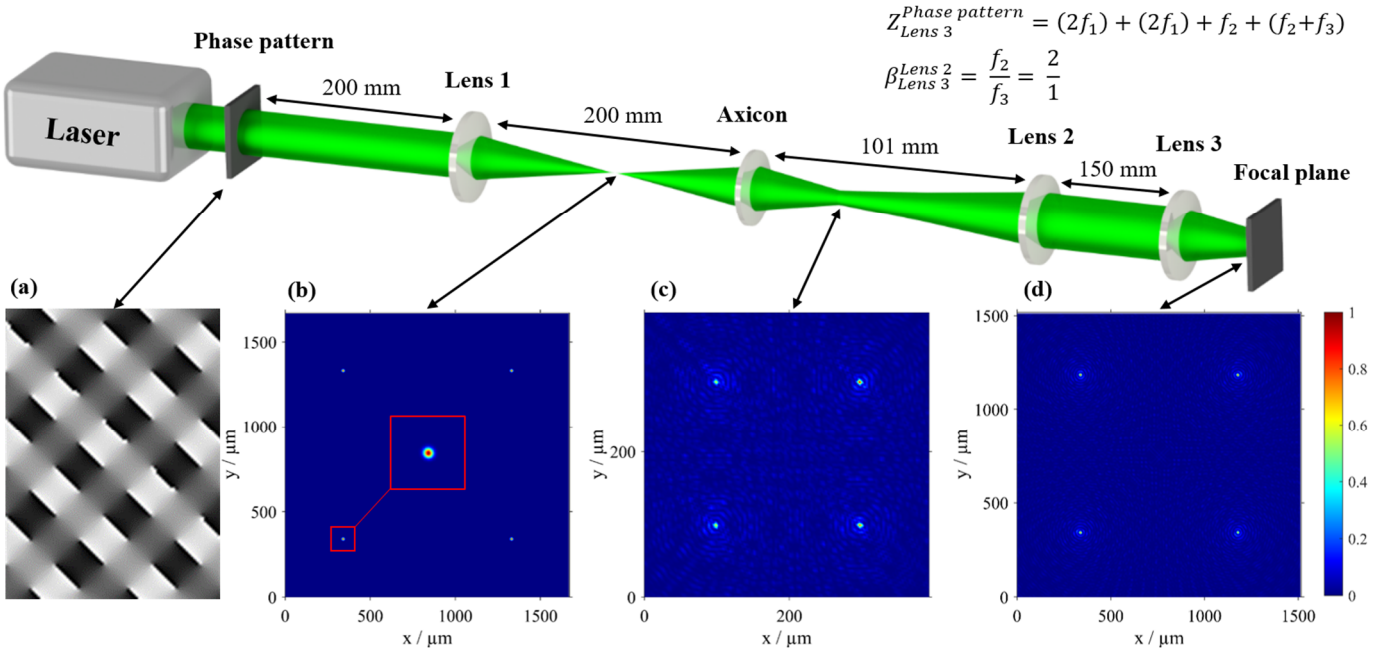

Figure 2. Schematic illustration of the simulated beam path including an SLM with a 4f-telescope and an axicon with a following imaging setup. Additionally, beside the shown phase pattern (**a**), the multi-spot beam profile in the intermediate focus (**b**), and the multi-Bessel beam after the axicon (**c**) as well as after the imaging setup (**d**) are shown. While the variable $z_{Lens\ 3}^{Phase\ pattern}$ in the shown formula defines the propagation distance of the beam path between the SLM and lens 3, $\beta_{Lens\ 3}^{Lens\ 2}$ indicates the magnification of lens 2 and 3.

While for the simulation results in Figure 3, the SLM was used only as a mirror, with respect to an exemplifying application in material processing, a binary-blazed grating is now applied to create a 2 × 1 beam splitter on the SLM. The binary-blazed grating has a periodical length of 16 pixels. In Figure 4, beam profiles are shown with the generated multi-Bessel beam at different propagation positions in 4 mm steps from 5 mm to 17 mm. For better visualization, the beam profiles shown in Figure 4 are normalized. As can be seen, the two generated Bessel beams distribute symmetrically, moving away from the center of the beam profile with continuous propagation. While the distance between the beams in the 5 mm position is 53 µm and increases to 182 µm at a propagation distance of 17 mm, showing that the two beams are arranged at an angle of 0.62° in relation to the propagation axis. It can also be seen that the Bessel beams are surrounded by diffraction patterns, which also separate with increasing propagation. However, it is obvious that

the two Bessel beams have the same intensity in the simulation, which predicts the ideal position of the components.

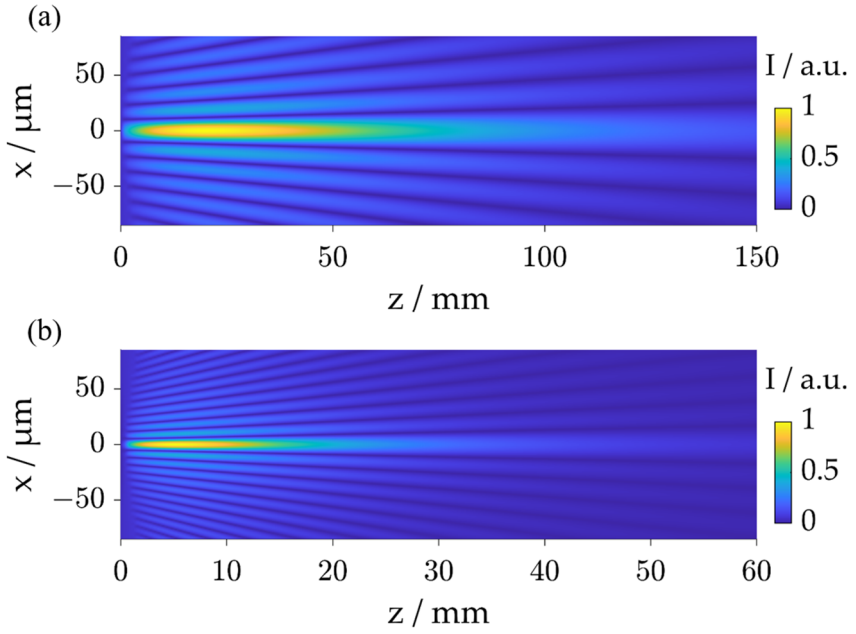

Figure 3. Simulated intensity distribution of the Bessel beam in propagation direction behind the axicon (**a**) and lens 3 (**b**).

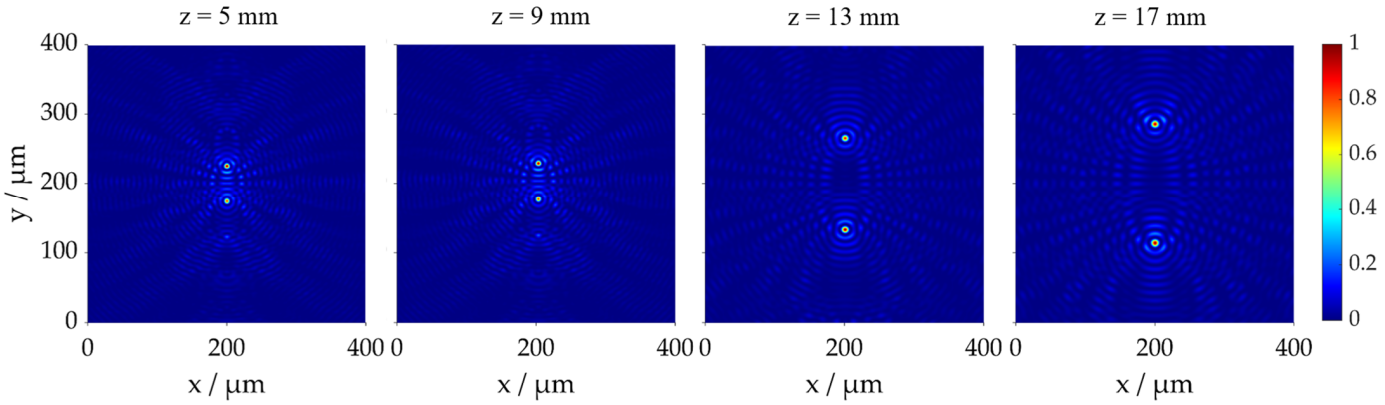

Figure 4. Simulated lateral intensity distributions of the multi-Bessel beam in the focal plane after lens 3 is taken in different z-axis positions from 5 mm to 17 mm in 4 mm steps.

4. Experimental Results

As illustrated in Figure 1, based on the simulation results, the optical setup is transferred to an optical breadboard to realize module integration into an existing ultrashort pulsed laser machine. To evaluate the optical simulation, the imaged workpiece was replaced by a camera, a neutral density filter with a transmission of 1% and a re-imaging lens setup for the detection of the lateral intensity profiles, which can be moved precisely along the propagation of the laser beam due to the installed axis with a length of 60 mm. For precise imaging of the experimentally generated Bessel beam, the camera is moved in steps of 250 µm by a motorized axis. For the single Bessel beam, the sequence of intensity distributions recorded in this way is shown in Figure 5. Due to the experimental measurements by a camera and the approach of different z positions in 250 µm steps, a lower resolution results in the diagram shown compared to the simulation. Due to the sequencing of the recorded beam profiles, pixel-wise positional errors occur, causing the intensity distribution in the propagation to exhibit slight fluctuations. Nevertheless, Figure 5 highlights that

the intensity distribution of the experimentally generated Bessel beam corresponds to the simulation and has a length of about 16 mm with a diameter of 6.4 µm at the peak of the highest intensity. The intensity maximum is approximately beyond a propagation length of 6 mm. In general, it can be stated that the beam-shaping results correspond well to the simulated results, apart from minor error influences.

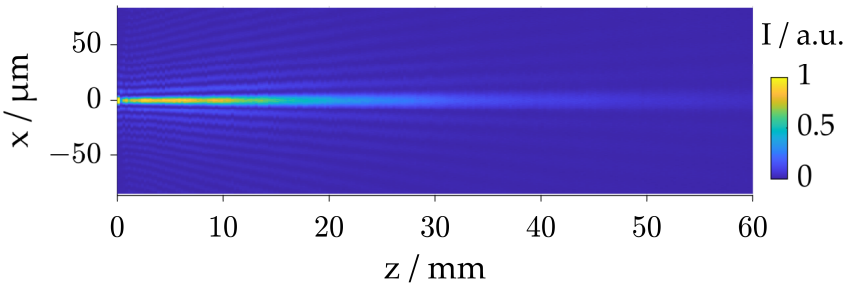

Figure 5. Measured intensity distribution in propagation direction of the Bessel beam behind lens 3.

In addition, we measured the multi-Bessel beam profiles at different positions behind lens 3 with an IDS camera in accordance with Figure 4. As shown in Figure 6 the Gaussian input beam with a diameter of 3.4 mm results in a 2 × 1 multi-beam with 88 µm separation, 5 mm behind lens 3. As already shown in the simulation, the Bessel beams deviate from a parallel course to the propagation axis so that they reach a separation of 258 µm after 17 mm propagation. The resulting angle is 0.81°, which is 0.2° larger than in the simulation. It can also be seen that the two Bessel beams are not identical, but they have slightly different intensities, which is particularly evident in the 5 mm and 13 mm positions. This may result from a slight misalignment and non-ideal optical components.

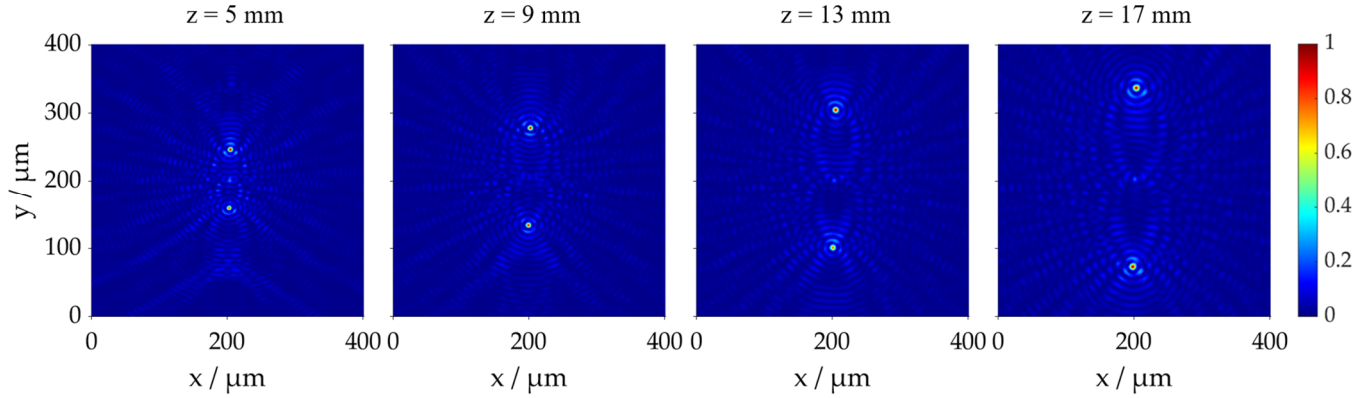

Figure 6. Measured lateral intensity distributions of the multi-Bessel beam in the focal plane after lens 3 taken in different z-axis positions from 5 mm to 17 mm in 4 mm steps.

In both the simulation and the experimental setup, diffraction effects occur due to the superposition of the SLM phase pattern and the axicon. Additionally, Orlov et al. [22] reported these interferences for beams with smaller separations. For example, a 2 × 1 Bessel beam profile with a separation of about 800 µm shows strong interference patterns, whereas with a double-sized separation, no interferences can be detected. Another effect is the visibility of the zeroth order in the center of the beam profile, which does not occur in the simulation results because an ideal diffraction element is used.

5. Drilling Study

To exemplify and initially demonstrate the experimental applicability of the multi-Bessel beam, a drilling study is performed on 5 µm-thin aluminum foils. The maximum average power of 10 W at a repetition rate of 50 kHz and a pulse duration of 220 fs was used to generate the drill holes. To achieve better drilling results in terms of the heat

effects, a pulse divider of five was used. Due to power losses in the numerous optical elements as well as the SLM, the measured power in the machining plane is 7 W. During the study, the number of pulses varied between 200 and 200,000. For the analysis of the six boreholes drilled with the 2 × 1 Bessel beam per parameter, the diameter of the boreholes was measured by two perpendicular lines and the averages were calculated from them. The output diameter is shown in Figure 7a for the different pulse numbers.

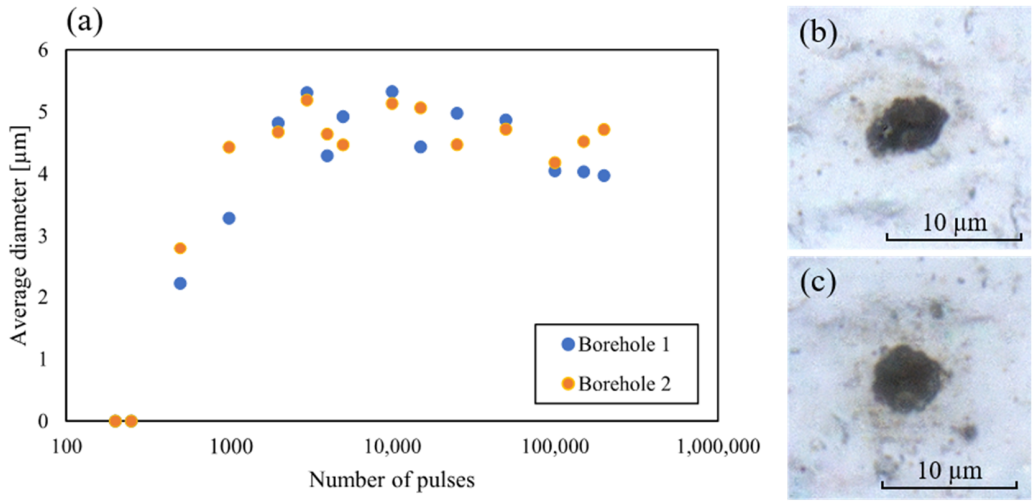

Figure 7. (**a**) Average diameter of the two holes drilled by a multi-Bessel beam as a function of the used number of pulses. The diameter is averaged through six drill holes, which were measured in x and y directions at an angle of 90 degrees. Please note, the standard deviation, of the measured quantities is in the order of 0.7 µm and is thus not considered in the diagram. (**b**) Outlet of a with 1000-pulse-drilled holes. (**c**) Outlet of with 10,000-pulse-drilled holes.

The first holes where the backside of the material is breached can be seen after about 500 pulses, although the holes are still very deformed and thus have a low roundness, as is visible in Figure 7b. This circumstance is commonly observed for drilling non-transparent materials using Bessel beams and is already known from other publications [18,19,31]. The initial diameter increases as a result of a higher pulse number of 2000 pulses to a maximum of approx. 5 µm, whereby the roundness of the holes increases significantly, as can be seen in Figure 7c. A further increase in the number of pulses leads to a stagnation of the initial diameter. The diameter of the drilled holes is about 5 µm, starting from a pulse number of 2000 with a measured diameter of the beam profile of 6.4 µm (FWHM) at the intensity maximum, according to Figure 5.

It is also evident that the diameter of borehole 2 in the boundary region of the breakthrough is slightly larger than that of borehole 1, indicating a slightly higher fluence in this Bessel beam. This may be due to a small misalignment in the beam path. However, the diameters converge significantly ay about 2000 pulses and vary for increasing pulse numbers in the same range.

6. Conclusions

We have developed and demonstrated the full functionality of an optical setup for generating multi-Bessel beams using a spatial light modulator and an axicon. To investigate the propagation properties of the generated Bessel beams, the system was simulated and experimentally characterized, where the calculated beam profiles with a length of approx. 17 mm show a high agreement in diameter and intensity compared to the experimentally measured beam profiles with a length of approx. 16 mm. Additionally, the analysis of a multi-Bessel beam generated by a binary-blazed grating on the SLM shows a high agreement between the simulation and the experimental setup. However, a slight deviation in the separation of the Bessel beams results from a minor difference in angle between the

propagation axis and the Bessel beams. A study on drilling thin aluminum foils with holes of a 5 µm outlet diameter shows the general applicability of the multi-Bessel beam module, which combines the possibility of flexible spot separation using customized phase patterns with the possibility of large axicon angles to generate small Bessel beams. These advantages enable high-throughput micromachining using multi-Bessel beams for drilling applications.

Author Contributions: Conceptualization, C.L. and S.S.; methodology, C.L., S.S. and R.H.; software, C.L. and S.S.; validation, C.L.; formal analysis, C.L.; investigation, C.L.; data curation, C.L.; writing—original draft preparation, C.L. and R.H; writing—review and editing, C.L., S.S., J.M., C.E. and R.H.; visualization, C.L. and S.S.; supervision, C.E. and R.H.; project administration, C.E. and R.H.; funding acquisition, R.H. All authors have read and agreed to the published version of the manuscript.

Funding: We gratefully acknowledge funding by the German Federal Ministry for Economic Affairs and Climate Action (grant 16KN053049) and of the Bavarian Research Foundation (grant AZ-1554-22).

Data Availability Statement: Data available on request due to restrictions, e.g., privacy or ethical. The data presented in this study are available on request from the corresponding author.

Conflicts of Interest: The authors declare no conflict of interest.

References

1. Durnin, J. Exact solutions for nondiffracting beams I The scalar theory. *J. Opt. Soc. Am. A* **1987**, *4*, 651–654. [CrossRef]
2. Durnin, J.; Miceli, J.; Eberly, J. Diffraction-free beams. *Phys. Rev. Lett.* **1987**, *58*, 1499–1501. [CrossRef]
3. Brzobohatý, O.; Cizmár, T.; Zemánek, P. High quality quasi-Bessel beam generated by round-tip axicon. *Opt. Express* **2008**, *16*, 12688–12700. [CrossRef]
4. Xie, Q.; Li, X.; Jiang, L.; Xia, B.; Yan, X.; Zhao, W.; Lu, Y. High-aspect-ratio, high-quality microdrilling by electron density control using a femtosecond laser Bessel beam. *Appl. Phys. A* **2016**, *122*, 136. [CrossRef]
5. Tiwari, S.K.; Mishra, S.R.; Ram, S.P.; Rawat, H.S. Generation of a Bessel beam of variable spot size. *Appl. Opt.* **2012**, *51*, 3718–3725. [CrossRef]
6. Schwarz, S.; Rung, S.; Esen, C.; Hellmann, R. Fabrication of a high-quality axicon by femtosecond laser ablation and CO_2 laser polishing for quasi-Bessel beam generation. *Opt. Express* **2018**, *26*, 23287–23294. [CrossRef]
7. McGloin, D.; Dholakia, K. Bessel beams: Diffraction in a new light. *Contemp. Phys.* **2005**, *46*, 15–28. [CrossRef]
8. Zhang, H. Lens axicons illuminated by Gaussian beams for generation of uniform-axial intensity Bessel fields. *Opt. Commun.* **2000**, *39*, 803. [CrossRef]
9. McLeod, E.; Hopkins, A.B.; Arnold, C.B. Multiscale Bessel beams generated by a tunable acoustic gradient index of refraction lens. *Opt. Lett.* **2006**, *31*, 3155–3157. [CrossRef]
10. Vijayakumar, A.; Bhattacharya, S. Phase-shifted Fresnel axicon. *Opt. Lett.* **2012**, *37*, 1980–1982. [CrossRef]
11. Chattrapiban, N.; Rogers, E.A.; Cofield, D.; Hill, W.T.; Roy, R. Generation of nondiffracting Bessel beams by use of a spatial light modulator. *Opt. Lett.* **2003**, *28*, 2183–2185. [CrossRef]
12. Bhuyan, M.K.; Courvoisier, F.; Lacourt, P.-A.; Jacquot, M.; Furfaro, L.; Withford, M.J.; Dudley, J.M. High aspect ratio taper-free microchannel fabrication using femtosecond Bessel beams. *Opt. Express* **2010**, *18*, 566–574. [CrossRef]
13. Bowman, R.; Muller, N.; Zambrana-Puyalto, X.; Jedrkiewicz, O.; Di Trapani, P.; Padgett, M.J. Efficient generation of Bessel beam arrays by means of an SLM. *Eur. Phys. J. Spec. Top.* **2011**, *199*, 159–166. [CrossRef]
14. Zhai, Z.; He, X.; Yu, X.; Liu, D.; Lv, Q.; Xiong, Z.; Wang, X.; Xu, Z. Parallel Bessel beam arrays generated by envelope phase holograms. *Opt. Lasers Eng.* **2023**, *161*, 107348. [CrossRef]
15. Stoyanov, L.; Zhekova, M.; Stefanov, A.; Stefanov, I.; Paulus, G.G.; Dreischuh, A. Zeroth- and first-order long range non-diffracting Gauss-Bessel beams generated by annihilating multiple-charged optical vortices. *Sci. Rep.* **2020**, *10*, 21981. [CrossRef]
16. Dudutis, J.; Gečys, P.; Račiukaitis, G. Non-ideal axicon-generated Bessel beam application for intra-volume glass modification. *Opt. Express* **2016**, *24*, 28433–28443. [CrossRef]
17. Mitra, S.; Chanal, M.; Clady, R.; Mouskeftaras, A.; Grojo, D. Millijoule femtosecond micro-Bessel beams for ultra-high aspect ratio machining. *Appl. Opt.* **2015**, *54*, 7358–7365. [CrossRef]
18. Alexeev, I.; Leitz, K.-H.; Otto, A.; Schmidt, M. Application of Bessel beams for ultrafast laser volume structuring of non transparent media. *Phys. Procedia* **2010**, *5*, 533–540. [CrossRef]
19. He, F.; Yu, J.; Tan, Y.; Chu, W.; Zhou, C.; Cheng, Y.; Sugioka, K. Tailoring femtosecond 1.5-µm Bessel beams for manufacturing high-aspect-ratio through-silicon vias. *Sci. Rep.* **2017**, *7*, 40785. [CrossRef]
20. Boucher, P.; Hoyo, J.D.; Billet, C.; Pinel, O.; Labroille, G.; Courvoisier, F. Generation of high conical angle Bessel-Gauss beams with reflective axicons. *Appl. Opt.* **2018**, *57*, 6725–6728. [CrossRef]
21. Dudutis, J.; Stonys, R.; Račiukaitis, G.; Gečys, P. Aberration-controlled Bessel beam processing of glass. *Opt. Express* **2018**, *26*, 3627–3637. [CrossRef]

22. Orlov, S.; Juršėnas, A.; Baltrukonis, J.; Jukna, V. Controllable Spatial Array of Bessel-like Beams with Independent Axial Intensity Distributions for Laser Microprocessing. *J. Laser Micro Nanoeng.* **2018**, *3*, 324–329.
23. Schwarz, S.; Rung, S.; Esen, C.; Hellmann, R. Rapid fabrication of precise glass axicon arrays by an all laser-based manufacturing technology. *J. Laser Appl.* **2020**, *32*, 12001. [CrossRef]
24. Roth, G.-L.; Rung, S.; Esen, C.; Hellmann, R. Microchannels inside bulk PMMA generated by femtosecond laser using adaptive beam shaping. *Opt. Express* **2020**, *28*, 5801–5811. [CrossRef]
25. Lutz, C.; Roth, G.; Rung, S.; Esen, C.; Hellmann, R. Efficient Ultrashort Pulsed Laser Processing by Dynamic Spatial Light Modulator Beam Shaping for Industrial Use. *J. Laser Micro Nanoeng.* **2021**, *16*, 62–67.
26. García-Martínez, P.; Sánchez-López, M.M.; Davis, J.A.; Cottrell, D.M.; Sand, D.; Moreno, I. Generation of Bessel beam arrays through Dammann gratings. *Appl. Opt.* **2012**, *51*, 1375–1381. [CrossRef]
27. Cheng, H.; Xia, C.; Kuebler, S.M.; Golvari, P.; Sun, M.; Zhang, M.; Yu, X. Generation of Bessel-beam arrays for parallel fabrication in two-photon polymerization. *J. Laser Appl.* **2021**, *33*, 12040. [CrossRef]
28. Tao, S.H.; Yuan, X.-C.; Ahluwalia, B.S. The generation of an array of nondiffracting beams by a single composite computer generated hologram. *J. Opt. A Pure Appl. Opt.* **2005**, *7*, 40–46. [CrossRef]
29. Litvin, I.A.; Mhlanga, T.; Forbes, A. Digital generation of shape-invariant Bessel-like beams. *Opt. Express* **2015**, *23*, 7312–7319. [CrossRef]
30. Jezek, J.; Cizmár, T.; Nedela, V.; Zemánek, P. Formation of long and thin polymer fiber using nondiffracting beam. *Opt. Express* **2006**, *14*, 8506–8515. [CrossRef]
31. Humbelani Edzani, R. Laser Drilling of Metals and Glass Using Zero-Order Bessel Beams. Master's Thesis, University of the Western Cape, Cape Town, South Africa, December 2013.